

Assessment of different approaches to rock physics modeling: a case study from offshore

Nile Delta

M. Aleari*, F. Ciabbarri**

***University of Pisa, Earth Sciences Department, **EDISON RD&I**

Corresponding author: M. Aleari (mattia.aleardi@unipi.it)

Abstract

The estimation of a reliable rock-physics model (RPM) plays a crucial role in reservoir characterization studies. In this work we assess different methods in deriving a reliable RPM that will be used in conjunction with amplitude versus angle inversion for the characterization of a clastic reservoir located in offshore Nile delta. The reservoir zone is located in gas saturated sand channels surrounded by shale sequences within a depth interval ranging between 2300 and 2700 m. A theoretical and three empirical approaches to derive a RPM are analyzed: the theoretical RPM is established using the well-known rock-physics equations valid for granular materials, whereas the empirical RPMs are derived using a multi-linear stepwise regression and two non-linear regression procedures based on neural networks (NN) and genetic algorithms (GA). A proper calibration and validation of the derived RPMs is conducted by using the extensive log suite of four existing wells drilled over an area of 100 km². For the investigated reservoir interval and for the encasing shales all the analyzed methods gives a final RPM that is able to reliably predict the elastic attributes (P-wave, S-wave velocity and density) from the petrophysical properties of interest (porosity, water saturation, and shaliness). Among the empirical approaches, the RPM predicted by the multi-linear regression is characterized by a prediction capability very similar to the RPMs predicted by the non-linear GA method, thus demonstrating that in the investigated zone the relation linking the petrophysical properties to the elastic attributes can be conveniently described by a multi-linear model. Differently the NN method seems to be affected by the overfitting problem that produces a RPM with less prediction capability than the RPMs estimated by the other methods. For what

concerns the theoretical method it produces a final estimates very similar to those produced by the multi-linear regression.

Introduction

Reservoir characterization studies provide rock property maps for field appraisal, selection of optimal well location, and production enhancement (Bosh et al. 2010). Seismic-reflection data are often used for reservoir characterization not only for obtaining a geometric description of the main subsurface structures but also for estimating properties such as lithologies and fluid contents at the target levels. To this end, a rock-physics model (RPM) is often incorporated into a seismic inversion scheme, such as amplitude versus angle (AVA) inversion (Mukerji et al.2001; Eidsvik et. al 2004; Bosh et al. 2007; Grana and Della Rossa, 2010; Bosch et al. 2015) or full-waveform inversion (Bacharach, 2006) to directly derive petrophysical rock properties from pre-stack seismic reflection data. This inversion process is usually referred to as the seismic-petrophysical inversion (Coléou et al. 2005).

A RPM is a generic relation (f_{RPM}) that can be expressed as follow:

$$[V_p, V_s, Density] = f_{RPM}(\phi, S_w, Sh, z) \quad (1)$$

It links petrophysical rock properties (which in case of clastic lithologies typically are porosity - ϕ -, water saturation - S_w - , shale content - Sh -) to elastic attributes (such as P-wave and S-wave velocities - V_p , V_s - and density) within the depth level of interest (z). Equation 1 can be based on a theoretical model (Avseth et al. 2005; Mavko et al. 2009), or on empirical relation derived from available well-log data or core measurements by means of a regression procedure (Mazzotti and Zamboni, 2003; Chiappa and Mazzotti, 2009). In the last case, either a linear or a non-linear rock-physics model can be considered (Han, 1986; Eberhart-Phillips et al. 1989).

Establishing an appropriate RPM deserves special attention in the case of seismic-petrophysical inversion. Many and very different inversion algorithms/approaches have been proposed to derive petrophysical rock properties from seismic data. These approaches go from simple deterministic

linear or non-linear inversions, to probabilistic inversions with different assumptions about the prior distributions, and to other even more complex inversion algorithms that try to incorporate as many prior information (e.g. geostatistical information) and as many experimental data (e.g. joint inversion) as possible to better constrain the final results. However, it is evident that any inversion method would fail if the RPM has a suboptimal prediction capability. For this reason, the present paper focuses on the derivation of a reliable RPM and presents a case history in which four different approaches to rock-physics modeling are investigated in the context of a clastic, gas-saturated reservoir in offshore Nile Delta. One of the reasons that motivate this study is that, at the best of our knowledge, it is not common to find publications in which different approaches to rock physics modeling have been discussed and compared based on the same reservoir data.

The investigated field is located in the offshore Nile delta and covers an area of approximately 100-km² in the Abū Qīr bay, off the coast of Alexandria (Egypt). The targets are gas-bearing sands at the depth range of 2300-2700 m that pertain to slope-channel systems of Plio-Pleistocene age. Layering is typically on the centimeter scale, and the reservoir mainly consists in rather clean-sand layers interbedded with laminated non-permeable shales, whereas in localized portions the sand bodies are characterized by a lesser amount of limestone and anhydrite that will be excluded from the derivation of the rock-physics models.

We consider three empirical methods and the well-known approach based on the theoretical formulas known as Hertz-Mindlin model, Hashin-Strickmann bounds and Gassmann equations, valid for granular materials (Mavko et al. 2009). The empirical approaches we consider are a multi-linear stepwise regression and two non-linear regression procedures driven by neural networks and genetic algorithms. We start by introducing the different methods used to derive the theoretical and the empirical RPMs. Then, after a brief overview of the geological setting of the investigated area, we appraise the estimated RPMs by comparing the actual versus the predicted elastic properties, by analyzing the correlation coefficients between the estimated and the actual recorded elastic properties and by performing a series of blind tests. Moreover, the RPMs resulting from theoretical

and empirical approaches are analyzed in detail to define the benefits and the limits of each method. We also discuss the differences between linear and non-linear methods for the specific case under examination, and we analyze the possible drawbacks that affect the neural network technique.

A brief introduction to the methods used for deriving the rock-physics models

In this chapter we briefly describe the empirical and the theoretical methods tested in this study to derive the RPMs. For each method we indicate appropriate references to the reader interested in additional details. We start with the multi-linear stepwise regression followed by the genetic algorithm optimization and the neural network method that have been used in the empirical approach. The theoretical approach to the definition of a RPM will be introduced thereafter.

Multi-linear stepwise regression

Stepwise regression (*SR*) is a semi-automated process of deriving a linear equation by successively adding or removing variables in the regression procedure based solely on the *t*-statistics of their estimated coefficients (Draper and Smith 1985). Using the multi-linear *SR* the equation describing the RPM can be written as follows:

$$EP = k + \sum_{n=1}^N a_n PP_n + bz \quad (2)$$

where the vector *EP* represents an elastic property (*V_p*, *V_s* or density), *PP* is the vector containing a generic petrophysical property (*φ*, *S_w* or *S_h*) and *N* is the total number of petrophysical properties considered in the regression process. The intercept term (*k*), the *b* term that describe the depth influence, and the weight of each input petrophysical properties (*a*) can be determined by means of three approaches: forward selection, backward elimination and bidirectional elimination. The forward selection approach starts with no variable in the model (i.e. all coefficients *a*, *k* and *b* are set to zero) and proceeds forward (adding one variable at a time). The backward elimination starts with all potential variables in the model and proceeds backward (removing one variable at a

time). The bidirectional elimination, that is the approach used in this study, is essentially a forward selection procedure that allows to a selected variable to be eliminated or added at each optimization stage.

Genetic algorithm optimization

Genetic algorithms (GA) are a global stochastic optimization method based on the mechanics of natural selection and evolution according to the Darwinian principle of “survival of the fittest” (Holland, 1975). In a GA optimization procedure a population of randomly generated individuals, which represent candidate solutions to an optimization problem, is evolved toward better solutions applying three main genetic operators: selection, cross-over and mutation. More details can be found in Mitchell (1996) or Sivanandam and Deepa (2008).

Following Aleardi (2015), in the RPM estimation we apply a GA optimization to the following regression model:

$$EP = k + \sum_{n=1}^N a_n PP_n^{c_n} + bz \quad (3)$$

that is based on a generalization of classical depth trends (Banchs et al. 2001). The RPM described by Equation 3 differs from the RPM considered by step-wise regression (Equation 2) for the exponent c that is used to reproduce possible non-linear effects in the relation linking the petrophysical properties to the elastic attributes. In this work we apply a GA optimization in which a population of 100 individuals is evolved into 50 iterations. The unknown coefficients (k , a , b and c) are contained in each individual that is evolved during the GA optimization in which the L_2 norm between observed and predicted elastic properties defines the error function to be minimized.

Neural Network optimization

A neural network (NN) is a mathematical algorithm that mimics a central nervous system and can be trained to solve both classification problem (i.e. pattern recognition) and prediction problem

(i.e. interpolation problems) (Haykin, 1999). According to the type of training used, the NN can be classified into two main categories: supervised or unsupervised. An unsupervised NN learns to represent particular input patterns in a way that reflects the statistical structure of the overall collection of input patterns. In this procedure there are no explicit target outputs associated with each input. Conversely a supervised NN corresponds to a problem in which a set of input data and their corresponding outputs are available; in this way, the network can attempt to infer the relation that links the input and the output. Supervised neural networks provide a convenient framework for dealing with strongly nonlinear problems and they can be used to approximate any non-linear and continuous function if a sufficient number of input and corresponding output data is available (Bishop, 1995). In this work we use a supervised network, thus with the acronym NN we always refers to this type of algorithm.

Among the many different types of NN implementations the one that has found several applications in solving geophysical problems is the multilayer feed-forward neural network (Van der Baan and Jutten, 2000). The architecture of this network consists of one input layer, one output layer, and one or more hidden layers. The nodes (also called neurons) of each layer are connected with weights, and the nodes of the hidden layers can consist of non-linear or linear activation functions. The NN optimization is essentially a steepest descent algorithm that starts form randomly initialized weights that are iteratively adjusted using a technique called back-propagation (Haykin, 1999).

If we consider a single hidden layer with K neurons, N input nodes, and a single output node the final RPM given by the network can be written as:

$$EP = \sigma_o \left(\sum_{i=1}^K \sigma_h^i \left(k_i + \sum_{n=1}^N a_{i,n} PP_n + b_i z \right) \right) \quad (4)$$

Where σ_h and σ_o represent the activation functions associated with the K nodes in the hidden layer and with the output node, respectively. By comparing Equation 2, 3 and 4 emerges that the founding relations at the base of the SR, GA and NN approaches are similar. However, moving

from SR to GA and to NN more and more highly non-linear terms are progressively introduced in order to describe possible complex relations linking the petrophysical properties to the elastic attributes.

The sigmoid function is the activation function considered in this work. This is a continuously differentiable, monotonically increasing function that can be generically written as:

$$\sigma(x) = \frac{1}{1 + e^{-wx+b}} \quad (5)$$

Where x is an input vector, b represents the bias that shifts the sigmoid curve to the left or the right, and the weight w determines the slope of the sigmoid curve at the midpoint. The coefficients b and w for each node are computed such that the L_2 norm misfit between actual and predicted data is minimized. In this work, the output layer has a single node corresponding to a given elastic property, the input layer has 4 nodes (three for the petrophysical properties of interest and one for the depth), whereas 15 nodes form the single hidden layer we use. A schematic representation of this NN architecture is shown in *Figure 1*. For a review of neural networks and their geophysical applications see van der Baan and Jutten (2000), Poulton (2002) or Saggaf et al. (2003), whereas for more specific applications of the NN approach to derive a relation between petrophysical rock-properties and other attributes (such as seismic velocity, density, quality factors) see for example de Roos et al. (2001), Valenti (2009), Leite and Vidal (2011) or Parra et al. (2014).

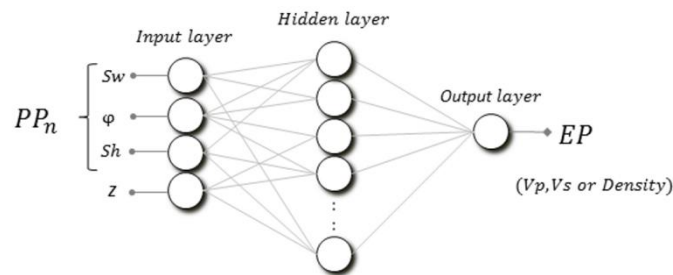


Figure 1: schematic representation of the NN architecture used in this work.

Theoretical rock-physics model

With theoretical rock-physics model (TRPM) we refer to one or more theoretical equations that establish a relationship between elastic attributes and petrophysical properties. To this end several models exist (e.g. granular media models and inclusion models). An extensive discussion of TRPM can be found in Mavko et al. (2009). In this work, following Avseth et al. (2005), we use the Hertz-Mindlin theory to define the shale and sand dry elastic properties at critical porosity and hydrostatic pressure, whereas the Hashin-Strikmann lower bound is used to simulate the compaction effect on the dry elastic moduli. The density and bulk modulus of gas and water are defined applying the Batzle and Wang equations (Batzle and Wang, 1992) taking into account temperature and pressure at the target depth. The properties of gas and water are combined according to the Wood equation (Mavko et al. 2009) to derive those of the saturating fluid. Finally, the Gassmann equation is used to combine the dry elastic properties of the rock matrix and the bulk modulus of the saturating fluid to compute the elastic moduli of the saturated rock. A schematic representation of this work-flow is represented in Figure 2. In the Nile delta province a temperature of approximately 60-65 °C characterizes the depth interval we investigate (2300-2700 m). This temperature is lower than the values of 130 °C at which starts the kaolinite-illite transformation and is also below the value of 75 °C at which starts the diagenetic transformation from smectite to illite that marks the boundary between the mechanical compaction regime and the transitional regime (Gouly and Ramdhan, 2012). For this reason, we consider a shale formed by a mix of smectite and kaolinite minerals and a not-cemented sand totally formed by quartz grains. The elastic moduli of clay minerals forming the shales, are highly variable (Avseth et al. 2005) since they are strongly influenced by mineral constituents, pore space microstructure, and orientations of clay platelets. Information about these variables is rarely available in real cases and thus the setting of reliable values for the elastic properties of clay is a very delicate issue when defining and calibrating a RPM. In this work, we have first averaged the values for the smectite and kaolinite elastic moduli reported in the literature (e.g. Brevik 1996; Mondol et al. 2007; Moyano et al. 2012). Then, the averages we obtained have

been slightly modified to improve the fitting with the observed V_p and V_s values. The principal parameters used in defining the theoretical rock-physics model are summarized in Table 1.

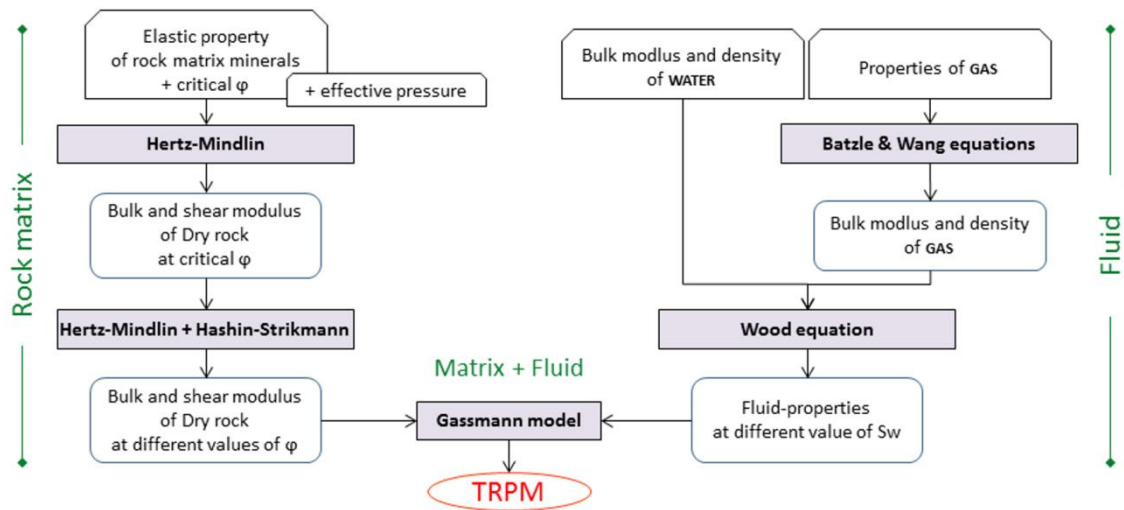


Figure 2: Schematic representation of the work-flow used to derive the theoretical RPM. The left side operations are used to derive the elastic properties of the dry rock, whereas the right side steps model the fluid properties. Then the Gassmann model combines the rock and the fluid properties to derive the elastic properties of the saturated rock.

<i>Quartz bulk modulus</i>	37 GPa
<i>Quartz shear modulus</i>	39 GPa
<i>Quartz density</i>	2650 Kg/m ³
<i>Clay bulk modulus</i>	13 GPa
<i>Clay shear modulus</i>	2 GPa
<i>Clay density</i>	2380 Kg/m ³
<i>Shale critical porosity</i>	70 %
<i>Sand critical porosity</i>	40 %
<i>Coordination number</i>	7
<i>Brine bulk modulus</i>	2.25 GPa

<i>Brine density</i>	1045 Kg/m ³
<i>Specific gas density</i>	0.9
<i>Temperature at the target depth</i>	65 °C

Table 1: The input parameters used in the definition of the theoretical RPM.

Results

In this chapter we analyze and comment the RPMs resulting from theoretical (TRPM) and from linear (SR) and non-linear (NN and GA) empirical approaches. The well-log data used to calibrate, estimate and validate the RPMs pertain to four exploration wells drilled through the reservoir zone (sand) and the encasing rocks (shale). The elastic (V_p , V_s , density) and the petrophysical (Sh , Sw , φ) properties we consider are derived from formation evaluation analysis of actual well-log measurements and have been subjected to an accurate outlier removal procedure. The few and localized logged intervals with a not negligible content of limestone and/or anhydrite (higher than 10%) have been removed from the set of well log data used in the calibration and validation processes. In deriving the following RPMs we consider the entire shale content and water saturation ranges (from 0% to 100%), whereas the depth interval is limited to the target sands and the encasing shales and ranges from 2300 to 2700 m, approximately. This significant depth range allows us to consider the depth as an independent variable in the empirical RPMs and to reliably estimate its influence on the elastic properties. Therefore, the empirical RPMs can be used to predict the V_p , V_s and density values for different depths of the considered reservoir interval.

Figure 3 shows an example of logged elastic and petrophysical properties for a single well that reached the target, gas saturated, sand. Note the finely layered shale-sand sequence and the strong decrease of water saturation (increase of gas saturation) and the corresponding decrease of V_p and density and increase of V_s that occur at the top of the target gas-sand located at 2450 m depth, approximately.

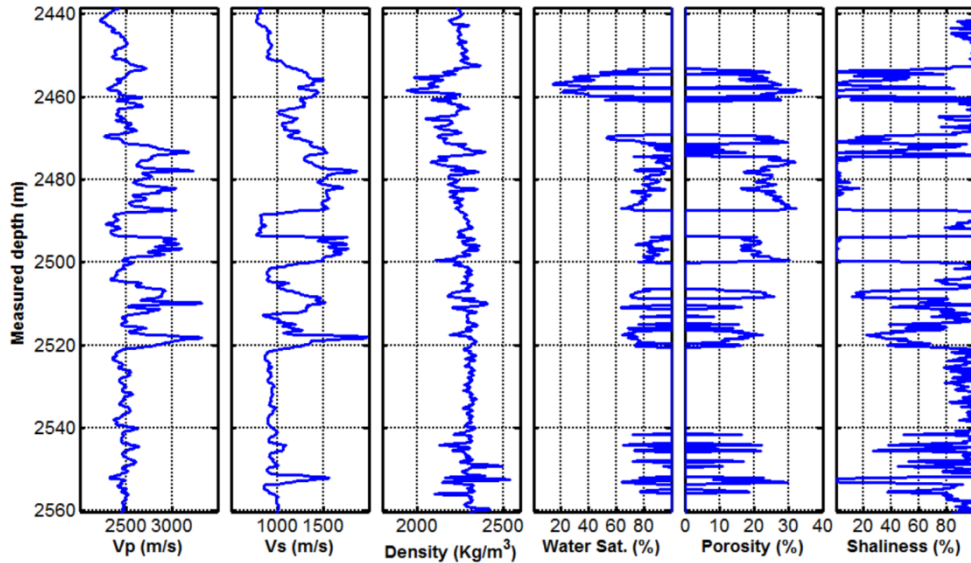


Figure 3: Examples of logged elastic properties and calculated petrophysical properties pertaining to a well that reached the reservoir rock. The top of the target gas-sand is located at 2450 m, approximately. From left to right: V_p , V_s , density, water saturation, porosity and shaliness.

A first assessment of the estimated RPMs can be done by comparing the measured elastic properties (from well-log), with those properties predicted by including the actual petrophysical data in the RPMs. Figure 4 shows this comparison together with the resulting correlation coefficients. In Figure 4a, Figure 4b and Figure 4c we show a close-up of only 1000 samples, representative of both sand and shale extracted from the entire set of more than 4000 well-log samples used in the regression and that yield the correlation coefficients illustrated in Figure 4d, Figure 4e and Figure 4f. First of all, we note that independently from the method applied (SR, NN, GA or TRPM) the prediction capability of the RPMs decreases passing from density (Figure 4a) to V_p (Figure 4b) and to V_s (Figure 4c). Indeed, as it is well known, the relation linking the density to the petrophysical properties is simpler than the relations linking these properties to V_p and V_s . The higher correlation coefficient obtained for V_p (Figure 4e) with respect to V_s (Figure 4f) can be explained by the low-performance of the logging tools in measuring the S-velocity, and then the lower reliability of the V_s measurements with respect to the V_p and the density ones. For the density

the four methods return very high correlation coefficients. Differently, for V_p and, particularly, for V_s the NN method yields final estimates with the highest correlation coefficients, whereas slightly lower correlation coefficient are obtained by the SR, GA and the TRPM methods. The slightly higher correlation coefficients obtained by the empirical methods with respect to the TRPM can be easily explained taking into account that the empirical approaches are data-driven procedures, that derive the RPM by means of a regression procedure of the actual petrophysical properties and elastic attributes. Conversely, the theoretical approach is a data-independent method based on equations with general validity. Among the empirical approaches, NN produces a slightly better match than SR and GA, whereas the non-linear GA method and the multilinear SR algorithm return very similar predictions. In Figure 4c note that the NN method has been the only one that correctly fit the measured V_s value in the interval between 270-370 samples, approximately.

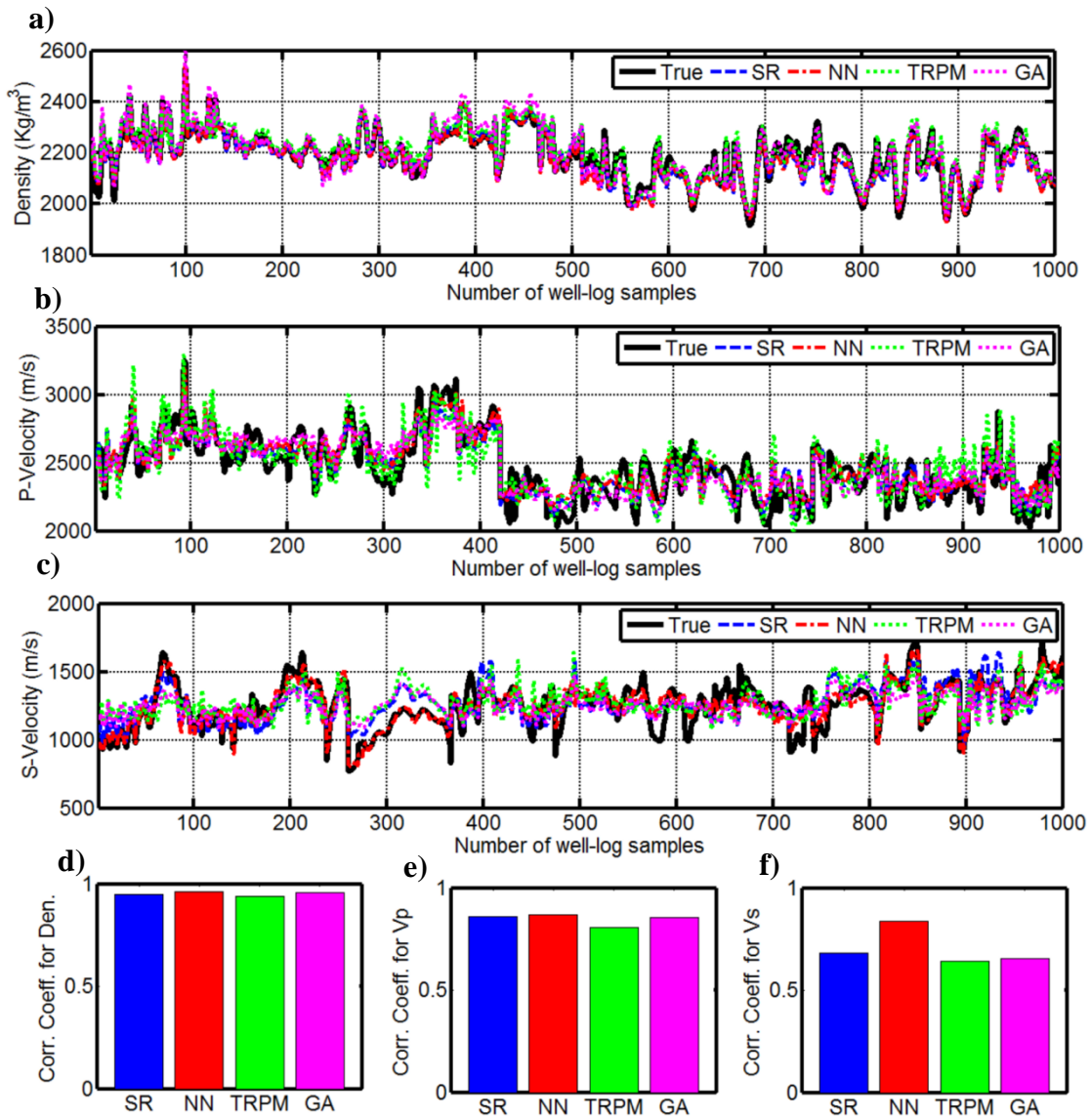


Figure 4: Comparison between the actual and the predicted elastic properties by the four RPMs. Density, V_p and V_s are represented in a), b) and c), respectively. The correlation coefficients computed for each approach are shown in d), e) and f) for density, V_p and V_s , respectively.

The main advantage of the SR and GA methods over the NN approach is that they directly provide final RPM equations with an easily interpretable rock-physical meaning. Conversely, with the NN method we derive a final equation that does not help us to infer anything about the physical meaning of the sought relation.

The SR approach returns the following RPM:

$$Vp[m/s] = 1732.3 + 0.542z + 1.647Sw - 28.742\phi - 9.056Sh \quad (6a)$$

$$Vs[m/s] = 1198.2 + 0.514z - 2.951Sw - 36.072\phi - 11.241Sh \quad (6b)$$

$$Density[Kg/m^3] = 2362.4 + 0.073z + 1.257Sw - 17.351\phi - 3.746Sh \quad (6c)$$

whereas with GA we obtain:

$$Vp[m/s] = 1685.5 + 0.623z^{0.94} + 1.831Sw^{1.16} - 30.142\phi^{0.87} - 8.547Sh^{1.04} \quad (7a)$$

$$Vs[m/s] = 1231.4 + 0.473z^{0.99} - 2.479Sw^{1.05} - 34.492\phi^{1.13} - 13.276Sh^{0.86} \quad (7b)$$

$$Density[Kg/m^3] = 2482.1 + 0.105z^{0.83} + 1.22Sw^{0.96} - 17.936\phi^{1.06} - 3.364Sh^{1.17} \quad (7c)$$

where the depth (z) is expressed in meters and Sw , ϕ and Sh in percentage. By comparing Equation 6 and 7, it emerges that the intercepts and the coefficients are very similar and, in addition, the exponents in Equation 7 are very close to one. These characteristics enable us to conclude that, in the specific case under examination, the relations linking the petrophysical to the elastic properties are close to be linear. This explains the very similar predictions returned by GA and SR, as previously evidenced in commenting Figure 4. Focusing our attention on the coefficients associated to the petrophysical variables we note that, as expected, Vp , Vs and density increase as the depth increases (the z parameter has always a positive coefficient), and decreases as the porosity increases (the ϕ parameter has always a negative coefficient); the Vp and density increases as the water saturation increases because gas is characterized by a lower bulk modulus (and density) than water (in Equations 6a, 6c and 7a, 7c, the Sw parameter has a positive coefficient). Conversely, the shear modulus is not affected by the saturating fluid and this fact, together with the density decrease produced by the increase of hydrocarbon saturation, explains the Vs increase as the water saturation decreases (in Equations 6b and 7b, the Sw parameter has a negative coefficient). The negative coefficients associated to Sh can be related to the reservoir depth interval we consider (2300-2700 m), characterized by a mechanical compaction regime. In this depth interval the Vp , Vs and the density of shales are lower than those of sands, as confirmed by a direct analysis of the well-log data (Figure 3). Finally, by comparing the magnitude of the coefficients, we conclude that the

porosity plays the major role in determining the elastic properties, followed by the shale content and the water saturation.

In Figure 5 we represent the so called rock-physics template (RPT) (Avseth et al. 2005). The RPT is a cross-plot that shows the influence of each petrophysical property on the elastic attributes P-impedance (I_p) and S-impedance (I_s). Figure 5a shows the RPT derived from the actual well-log data and the associated petrophysical properties. The hydrocarbon trend is also represented. As expected, we observe a decrease of I_p and an increase of I_s as the water saturation decreases and a decrease of both I_p and I_s with the increasing of porosity and shale content. These general trends are well matched by the RPTs derived from the empirical (Figure 5b, Figure 5c and Figure 5e) and the theoretical (Figure 5d) RPMs. As previously discussed, the RPTs estimated by GA and SR are very similar, and even in this case the NN method yields a better match with the actual RPT computed from actual well-log data. A slightly lower match characterizes the SR and the GA estimates and, particularly, the TRPM results.

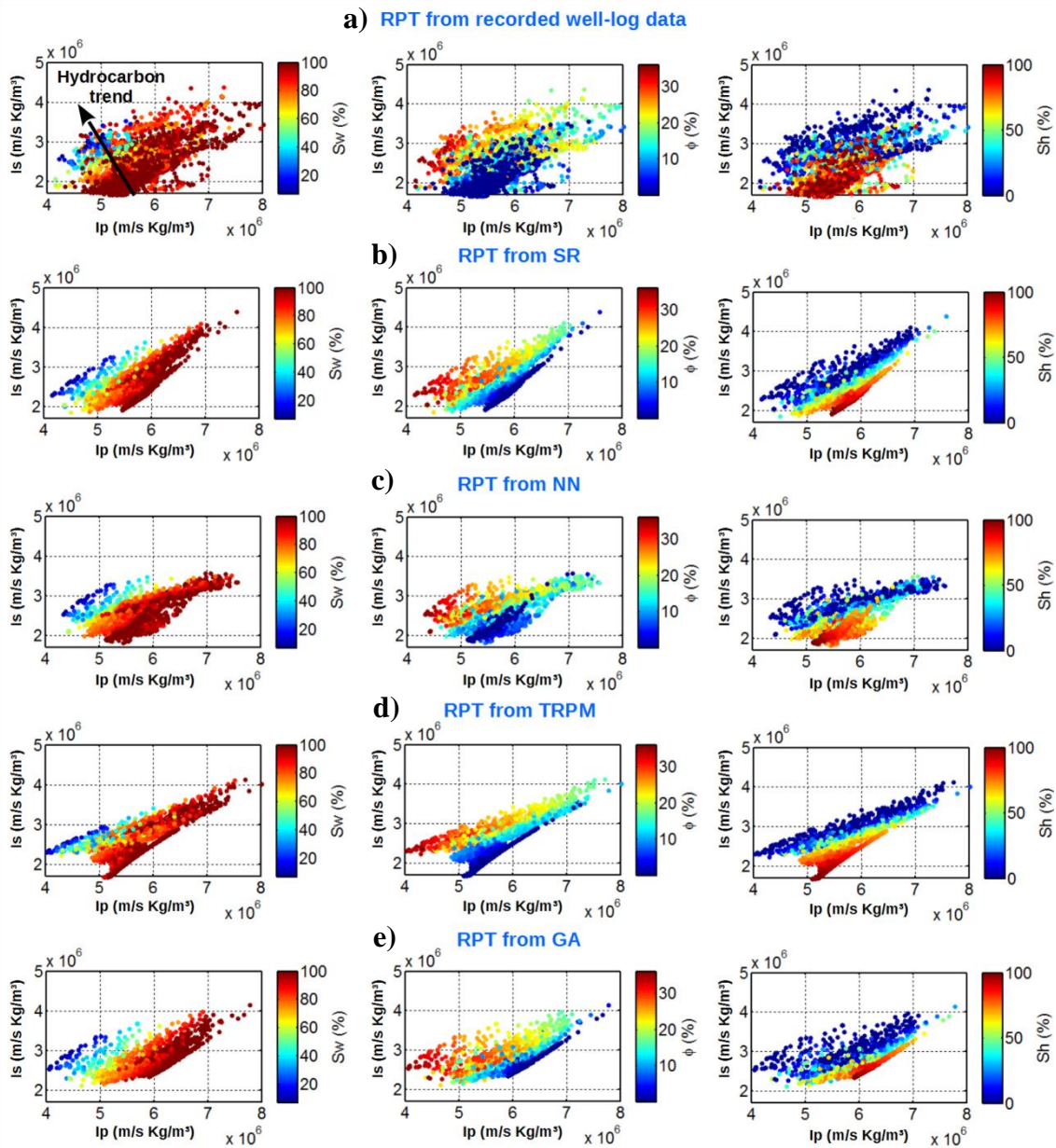


Figure 5: Rock-physic templates showing the influence of each petrophysical parameter on the P -impedance (I_p) and S -impedance (I_s). Water saturation (S_w), porosity (ϕ) and shaliness (Sh) are represented from left to right. Part a) refers to the actual well-log data, whereas parts b), c), d) and e) refer to the elastic properties predicted by the SR, NN, TRPM and GA methods, respectively.

In part a) the hydrocarbon trend is indicated by the black arrow.

The similarities and differences for each RPM can be better seen by performing a numerical analysis that allows for a graphical representation of the derived RPMs. In fact, the RPMs can be described as surfaces in a 5D space in which four orthogonal directions correspond to the independent variables (ϕ , S_w , Sh and z), and the fifth orthogonal direction can be either V_p or V_s or density. Such 5D surface can be also visualized in a 3D plot in which only two independent variables change, while the other two are considered fixed. For example, Figure 6 shows a graphical representation of the derived RPM for the V_s parameter as the porosity and shaliness vary while the water saturation and depth are kept constant at 50% and 2600 m, respectively. The great similarity between the SR and the GA results can be observed by comparing Figure 6a and Figure 6d. In addition, we note a fair similarity between the rock-physics models derived by the empirical SR and GA methods and the one resulting from the TRPM. All these three RPMs predict similar V_s increases with the decreasing of shale content and similar V_s increases as the porosity decreases. Conversely, the RPM obtained by the NN method is substantially different from the other ones: it shows an un-physical V_s decrease for a shaliness less than 40-50%, approximately. We interpret this fact as an overfitting problem that usually affects the NN method (van der Bann and Jutten, 2000). Generally speaking, overfitting occurs when a model describes random error or noise instead of the underlying relationship linking the input data to the output data. A model that has been overfitted will generally have poor predictive performance. This problem can be usually related to the architecture of the net used. However, not a unique rule exists to set the NN user-defined parameters (such as number of nodes, number of hidden layers or type of activation function). In addition neither theorem is able to predict the optimal number of neurons for a specific optimization procedure, although as indicated by Huang and Huang (1991) this number should never exceed the number of training samples. Usually, the best configuration is found by trial and error, starting with a small number of nodes and increase this number until the results does not change with increasing the number of neurons. Several methods are devoted to attenuate the overfitting problem, such as the early stopping criterion (van der Bann and Jutten, 2000), that has also been applied in this work.

However, in this specific case the early stopping criterion alone has not been able to completely prevent the overfitting problem. The overfitting associated with the NN method is also visible by comparing Figure 5a and Figure 5c, in which we observe that the RPT derived from the NN approach tends to reproduce the scatter visible in the RPT derived from the recorded logs. Since we have removed the lithological heterogeneities from the set of input data for the calibration and validation processes, we opt to ascribe this scatter to inaccurate measurements or to residual noise in the well-log data. In Figure 5 we can also appreciate that the theoretical RPM is characterized by the smallest scatter among the derived RPMs.

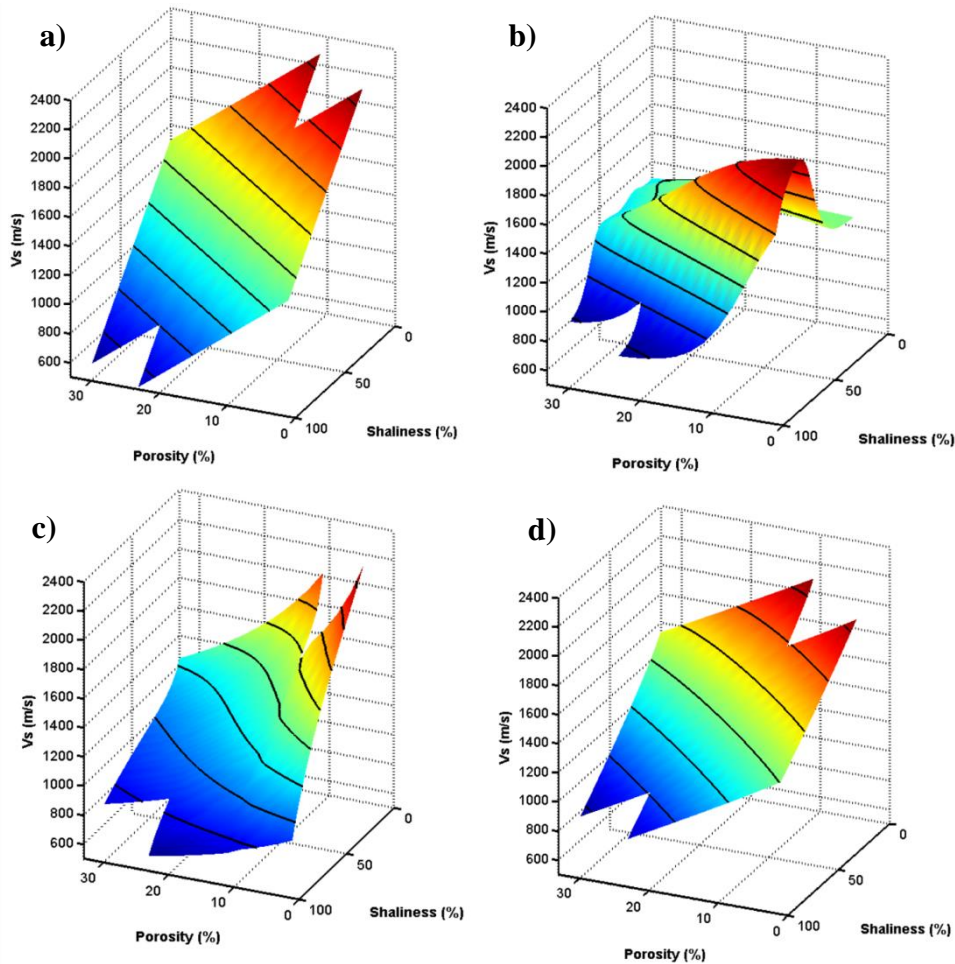


Figure 6: Graphical representations of the rock-physics models derived by step-wise regression, neural network, theoretical rock physics model and genetic algorithms are, respectively, shown in a), b), c) and d). These surfaces represent the V_s variations as a function of the shale content and the porosity, keeping fixed the depth and the water saturation to 2600 m and to 50%, respectively.

Figure 7 shows a graphical representation of the derived RPM for the V_p parameter as the porosity and water saturation vary while the shaliness and depth are kept constant at 20% and 2600 m. Also in this case we observe a great similarity between the outcomes derived by the SR, GA and the TRPM. The surfaces related to the SR, TRPM and GA clearly show the expected decrease of V_p as the porosity and water saturation decreases. As in Figure 6 the results of the NN method show complex and often unphysical V_p variations with porosity and water saturation changes. In particular, note the unphysical V_p decrease as the water saturation increases that occurs for a porosity range between 15% and 18% and the slight V_p increase as the porosity increase that occurs for a water saturation range between 80% and 100%. Finally, also note the unphysical V_p variations as the water saturation changes occurring for a porosity equal to 25%-30 %. We again interpret these unphysical V_p variations as an effect related to the overfitting problem.

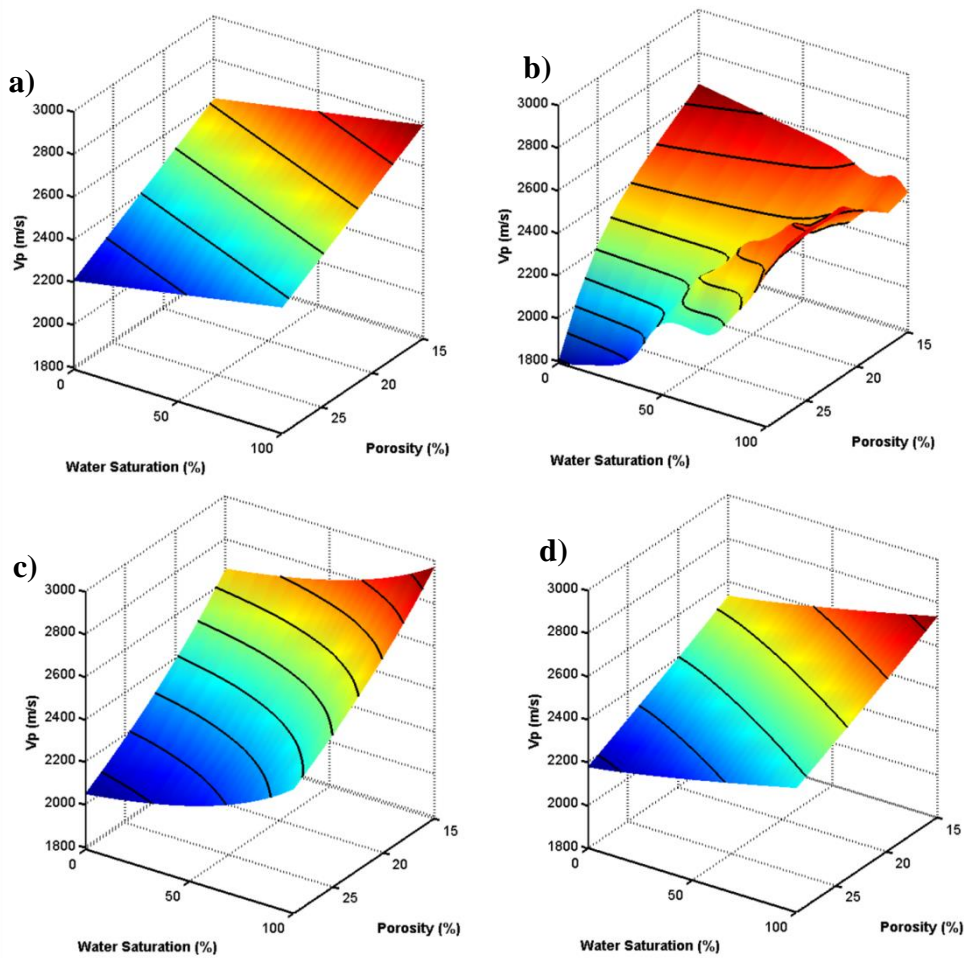


Figure 7: Graphical representations of the rock-physics models derived by step-wise regression, neural network, theoretical rock physics model and genetic algorithms are, respectively, shown in a), b), c) and d). These surfaces represent the V_p variations as a function of the water saturation and the porosity, keeping fixed the depth and the shaliness to 2600 m and to 20%, respectively.

Finally, if we compare the surface describing the density variations predicted by the four RPMs, we observe that a great similarity characterizes the outcomes of the different methods (Figure 8). This fact is another demonstration of the nearly linear relation that relates the density to the petrophysical rock properties. In this last example also the NN method generate a nearly flat surface and density variations that are comparable with those predicted by the other methods.

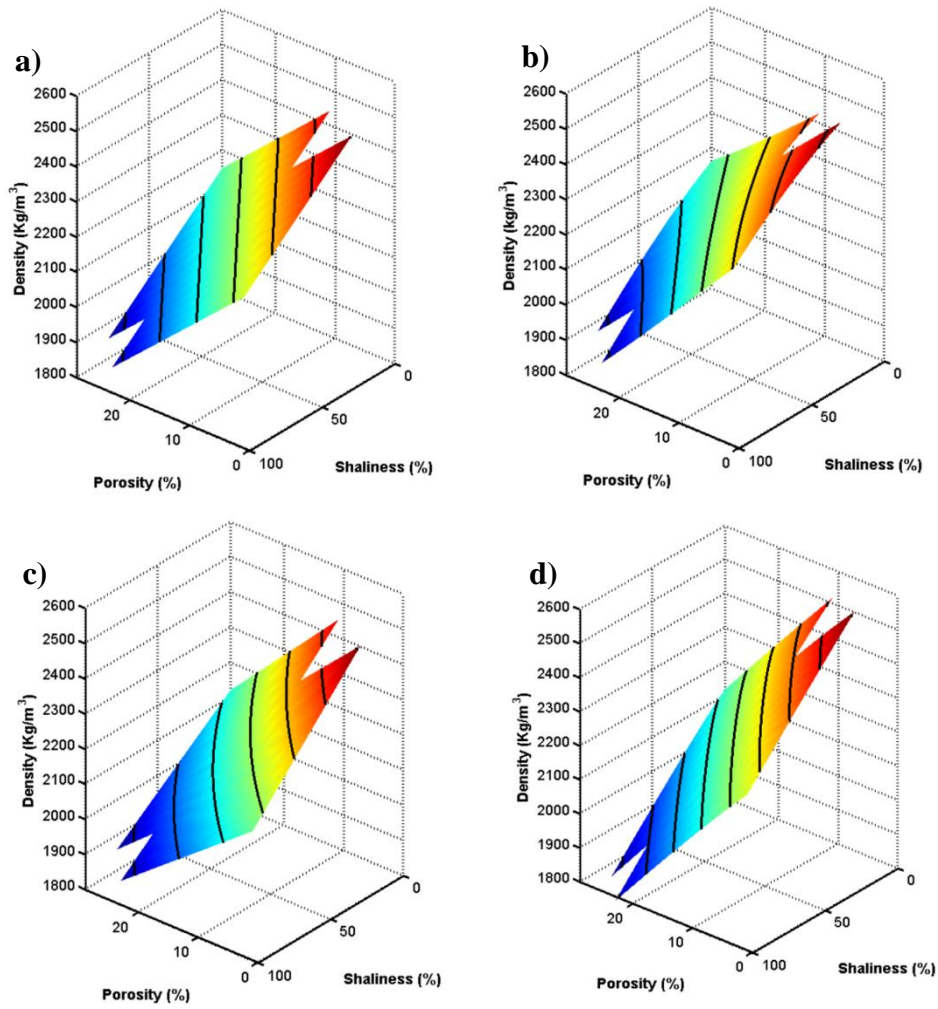


Figure 8: Graphical representations of the rock-physics models derived by step-wise regression, neural network, theoretical rock physics model and genetic algorithms are, respectively, shown in a), b), c) and d). These surfaces represent the density variations as a function of the shaliness and the porosity, keeping fixed the depth and the water saturation to 2600 m and to 50%, respectively.

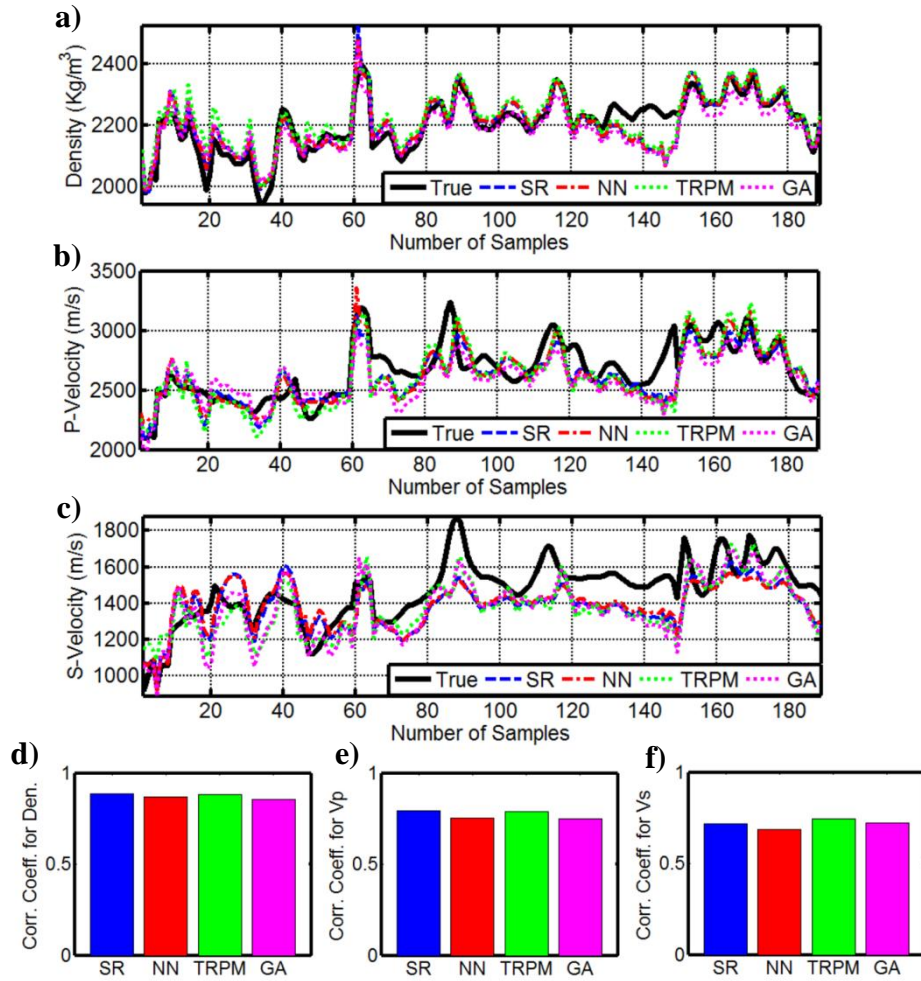


Figure 9: Results of the blind test. V_p , V_s and density are represented in a), b) and c), respectively. The correlation coefficients computed for each approach are shown in d), e) and f) for V_p , V_s and density, respectively.

To further assess the applicability and the reliability of the derived RPMs we perform a series of blind tests in which the petro-elastic relations expressed by the four RPMs are used to predict the elastic properties in a nearby well that was not used in the estimation process of the RPMs (Figure 9). This well was drilled in the same target area and through geological formations with similar characteristics. This test is also aimed at quantifying the prediction capability of each RMP. Figure 9 shows that, as expected, the prediction capability for each method decrease passing from the density (Figure 9a) to V_p (Figure 9b) and, particularly, to V_s (Figure 9c). We also note that, thanks to its general validity, the TRPM estimates show very high correlation coefficients with the actual

data. Conversely, the correlation coefficients associated with the empirical, data-driven, approaches are generally decreased with respect to the results obtained in the optimization procedure (see Figure 4). This blind test allows us to discuss a fundamental difference between the empirical and the theoretical approaches that explains the lower correlation coefficients that characterize all the empirical RPMs with respect to the theoretical one. Even if the input set of elastic and petrophysical properties, used in defining the rock-physics model, belong to wells drilled through geological formations with similar characteristics, the empirical, data-driven, approaches return slightly different models depending on the set of input data considered in the prediction procedure. This fact can be ascribed to errors and uncertainties that affects the measured elastic properties and to errors and approximations made in the formation evaluation analysis to derive the petrophysical properties. Differently, the TRPM result, being based on theoretical equations, is totally independent from errors and uncertainties in well-log measurements. Moreover, in this blind test the NN approach is always characterized by the lowest correlation coefficients, thus confirming that the overfitting problem is often associated with a sub-optimal prediction capability.

Another drawback of the NN method, not investigated here, is related to its local nature. In a NN optimization, the weights associated with each neuron are usually randomly initialized and are subsequently adjusted using a gradient-based strategy. This demonstrates the importance of a good initial model to prevent convergence towards a local minimum in the case of a complex multim minima error function. To attenuate this limitation, the NN optimization must be repeated many times starting from different initial models, from which the best result will be selected. This procedure can be very time consuming in the case of large numbers of training samples. Conversely, GA method (or other global search algorithms) circumvents this drawback by performing a wide and efficient exploration of the entire model space in a single inversion. These derivative-free, stochastic methods ensure that the final result is much less affected by multiple minima in the error function and by the choice of the initial model.

Conclusions

We have analyzed the rock-physics models (RPMs) obtained by applying both theoretical and empirical approaches. The fair match between the measured and predicted elastic properties and between the actual and the predicted RPTs demonstrates the potential of all the considered methods to yield final equations that are capable of estimating the elastic properties from a set of input petrophysical properties. The density estimates are characterized by very high correlation coefficients, whereas lower correlation coefficients characterize the predicted seismic P-wave and S-wave velocities. This result can be explained taking into account that the relation linking density to the petrophysical parameters is simpler than the relations existing between the petrophysical parameters and V_p and V_s . In addition, the lower correlation coefficient observed for the V_s estimates might be due to the lower performance of the logging tools in measuring the S-wave velocity.

We have shown that the non-linear GA and the linear SR methods return very similar equations, demonstrating that the relations linking the input petrophysical properties to the elastic attributes are, in this specific case, close to linear. This fact makes the application of an empirical non-linear method useless for the case under examination. However, in more complex geological scenarios the linear approach may not be enough to ensure a good match between measured and predicted properties. In these cases non-linear methods should be applied.

Among the non-linear methods we tested, an important limitation of the NN over the GA method is the overfitting problem and the difficulty that it is usually encountered in designing the NN architecture. Another drawback of the NN method is related to its local nature and to the need of a good initial model to prevent convergence towards local minima. A common approach to overcome this drawback consists in performing many NN optimizations starting from different initial models, and then considering as the final result the model with the minimum prediction error. In the particular application described in this work, we think that the main advantage of GA and SR over

NN is that they directly provide simple equations characterized by easily interpretable rock-physical meanings.

The blind test evidenced that the high correlation coefficients associated to the NN approach are likely related to the well-known overfitting problem. The blind test also demonstrated that the TRPM approach, thanks to its general validity, ensures very high prediction capabilities. Such high prediction capability and the general validity constitute the main advantages of the theoretical approach with respect to the empirical one. However, the very similar relations obtained in this specific case by the theoretical rock-physics approach and by the linear step-wise regression make the empirical method for deriving the RPM particularly attractive because it is very simple to calibrate and to implement. Therefore, the theoretical RPMs may not be necessary when dealing with simple geological and lithological contexts as the Plio-Pleistocenic formations in the Nile delta. In these cases the empirical approach to rock-physics modeling can be the fastest way of obtaining a model calibration suitable for reservoir characterization. In complex geologic scenarios (fractured rocks, non-clastic rocks, overpressured rocks, chemical compaction regimes) multiple parameters (e.g. parameters about the pore space microstructure and/or anisotropy parameters) must be taken into account and a deeper insight into the geological context are needed to define a RPM suitable for reservoir characterization. The consideration of all these variables and their complex interrelationships in an optimization procedure could make the empirical approach inapplicable. In these cases the theoretical formula could be the only way of obtaining a reliable RPM. It should be taken into consideration that the empirical approaches must be intended as strictly target-oriented approaches to rock-physics modeling. In other words, the RPM equation derived by applying an empirical method must be redefined for each different exploration target. This fact determines that the suitability of a RPM derived by an empirical approach is strongly case dependent. On the contrary a theoretical RPM is based on equations that offer a continuum-mechanics approximation of the elastic, or viscoelastic properties of rocks. Therefore, these theoretical equations should be able (in principle) to yield accurate predictions for every situations given that the assumptions made

in deriving the theoretical model are verified and being the input parameters to the theoretical formula (e.g. the elastic moduli of the mineral constituents and of the saturating fluid) in good agreement with the true ones. This is the main difference between the theoretical and the empirical approach to rock-physics modeling.

In conclusion, in the analyzed case, the simplicity of the empirical rock-physics model derived by applying multi-linear stepwise regression, and the reliability of the theoretical rock-physics equations make the outcome resulting from these two approaches the best candidates to play the role of RPM in the following seismic-petrophysical inversion that we performed in the next phase of the reservoir characterization study (Aleari et al. 2016a, 2016b). In particular, the possibility of describing the RPM by means of linear equations is particularly useful as it greatly simplifies the uncertainty propagation in the inversion. We are aware that the present paper can not constitute a complete overview of all the possible geologic scenarios that could be encountered in hydrocarbon exploration. However, the different approaches we presented are generally applicable to different scenarios and some conclusions we drew, although specifically valid for the analyzed case, could reveal to be of practical utility in similar geological contexts.

Acknowledgments

This study is a part of a collaborative research project between EDISON RD&I and the Earth Science Department of the University of Pisa. The authors wish to thank EDISON E&P for making the well-log data available and for the permission to publish this work and Prof. Alfredo Mazzotti for useful discussions and insightful comments.

References

- Aleardi, M., 2015, Seismic velocity estimation from well log data with genetic algorithms in comparison to neural networks and multilinear approaches: *Journal of Applied Geophysics*, 117, 13-22.
- Aleardi, M., Ciabbarri, F., Garcea, B., Peruzzo, F., and A. Mazzotti, 2016a, Probabilistic seismic-petrophysical inversion applied for reservoir characterization in offshore Nile delta: Expanded Abstract presented at the 78th EAGE Conference and Exhibition. DOI: 10.3997/2214-4609.201600969.
- Aleardi, M., Ciabbarri, F., Peruzzo, F., Garcea, B., and A. Mazzotti, 2016b, Bayesian Estimation of Reservoir Properties by Means of Wide-angle AVA Inversion and a Petrophysical Zoeppritz Equation. Expanded Abstract presented 78th EAGE Conference and Exhibition. DOI: 10.3997/2214-4609.201601551.
- Avseth, P., Mukerji, T., and G. Mavko, 2005, *Quantitative seismic interpretation: Applying rock physics tools to reduce interpretation risk*. Cambridge University Press.
- Bachrach, R., 2006, Joint estimation of porosity and saturation using stochastic rock-physics modeling: *Geophysics*, 71(5), O53-O63.
- Banchs, R., Jiménez, J., and E. Del Pino, 2001, Nonlinear estimation of missing logs from existing well log data: Expanded Abstract presented at the 71th SEG Annual Meeting, 598–600.
- Batzle, M., and Z. Wang, 1992, Seismic properties of pore fluids: *Geophysics*, 57(11), 1396-1408.
- Bishop, C., 1995, *Neural networks for pattern recognition*: Oxford University Press.
- Bosch, M., Cara, L., Rodrigues, J., Navarro, A., and M. Díaz, 2007, A Monte Carlo approach to the joint estimation of reservoir and elastic parameters from seismic amplitudes: *Geophysics*, 72(6), O29-O39.

Bosch, M., Mukerji, T., and E.F. Gonzalez, 2010, Seismic inversion for reservoir properties combining statistical rock physics and geostatistics: A review: *Geophysics*, 75(5), 75A165-75A176.

Bosch, M., Bertorelli, G., Álvarez, G., Moreno, A., and R. Colmenares, 2015, Reservoir uncertainty description via petrophysical inversion of seismic data: *The Leading Edge*, 34(9), 1018-1026.

Brevik, L., 1996, Inversion and analysis of Gassmann skeleton properties of shaly sandstones using wireline log data from the Norwegian North Sea: Expanded Abstract presented at the 66th SEG Annual Meeting, 130-133.

Chiappa, F., and A. Mazzotti, 2009, Estimation of petrophysical parameters by linearized inversion of angle domain pre-stack data: *Geophysical Prospecting*, 57(3), 413-426.

Coléou, T., Allo, F., Bornard, R., Hamman, J. G., and D.H. Caldwell, 2005, Petrophysical seismic inversion: Presented at the 75th SEG Annual Meeting, 1355-1358.

de Roos, M.C., Oldenziel, T., and C.P.J.W. van Kruijsdijk, 2001, Neural Network as an Alternative to Rock Physics Modeling in Time-Lapse Seismic Reservoir Monitoring. In *Offshore Technology Conference*. doi: 10.4043/13162-MS.

Draper, N.R., and H. Smith, 1985, *Applied Regression Analysis*: JohnWiley & Sons Inc.

Eberhart-Phillips, D., Han, D. H., and M.D. Zoback, 1989, Empirical relationships among seismic velocity, effective pressure, porosity, and clay content in sandstone: *Geophysics*, 54(1), 82-89.

Eidsvik, J., Avseth, P., More, H., Mukerji, T., and G. Mavko, 2004, Stochastic reservoir characterization using prestack seismic data: *Geophysics*, 69, 978–993.

Gouly, N.R., and A.M. Ramdhan, 2012, The challenge of pore pressure estimation in diagenetically consolidated mudrocks: *First Break*, 30(12).

Grana, D., and E. Della Rossa, 2010, Probabilistic petrophysical-properties estimation integrating statistical rock physics with seismic inversion: *Geophysics*, 75(3), O21-O37.

Han, D., 1986, Effects of porosity and clay content on acoustic properties of sandstones and unconsolidated sediments: Ph.D. dissertation, Stanford University.

Haykin, S., 1999, Self-organizing maps. *Neural Networks—A Comprehensive Foundation*: Prentice-Hall.

Holland, J.H., 1975, *Adaptation in Natural and Artificial Systems*: University of Michigan Press.

Huang, S.C., and Y.F. Huang, 1991, Bounds on the number of hidden neurons in multilayer perceptrons: *IEEE Transactions Neural Networks*, 2(1), 47-55.

Leite, E.P., and A.C. Vidal, 2011, 3D porosity prediction from seismic inversion and neural networks: *Computers & geosciences*, 37(8), 1174-1180.

Mazzotti, A., and E. Zamboni, 2003, Petrophysical inversion of AVA data: *Geophysical Prospecting*, 51(6), 517-530.

Mavko, G., Mukerji, T., and J. Dvorkin, 2009, *The rock physics handbook: Tools for seismic analysis of porous media*: Cambridge university press.

Mitchell, M., 1996, *An Introduction to Genetic Algorithms*: MIT Press.

Mondol, N.H., Bjørlykke, K., Jahren, J., and K. Høeg, 2007, Experimental mechanical compaction of clay mineral aggregates—Changes in physical properties of mudstones during burial: *Marine and Petroleum Geology*, 24(5), 289-311.

Moyano, B., Spikes, K.T., Johansen, T.A., and N.H. Mondol, 2012, Modeling compaction effects on the elastic properties of clay-water composites: *Geophysics*, 77(5), D171-D183.

Mukerji, T., Jørstad, A., Avseth, P., Mavko, G., and J.R. Granli, 2001, Mapping lithofacies and pore-fluid probabilities in a North Sea reservoir: Seismic inversions and statistical rock physics: *Geophysics*, 66, 988–1001.

Parra, J.O., Iturrarán-Viveros, U., Parra, J.S., and P.C. Xu, 2014, Neural network and rock physics for predicting and modeling attenuation logs. Expanded Abstract presented at the 84th SEG Annual Meeting, 633-637.

Poulton, M., 2002, Neural networks as an intelligence amplification tool: A review of applications: *Geophysics*, **67**, 979–993.

Saggaf, M., Toksöz N., and H.M. Mustafa, 2003, Estimation of reservoir properties from seismic data by smooth neural networks: *Geophysics*, 68, 1969–1983.

Sivanandam, S. N., and S.N. Deepa, 2008, *Genetic Algorithm Optimization Problems*: Springer Berlin Heidelberg.

Valenti, 2009, Porosity prediction from seismic data using multiattribute transformations, N Sand, Auger Field, Gulf of Mexico: MS thesis, Pennsylvania State University.

Van der Baan M., and C. Jutten, 2000, Neural networks in geophysical applications: *Geophysics* 65 (4), 1032–1047.

Captions

Figure 1: Schematic representation of the NN architecture used in this work.

Figure 2: Schematic representation of the work-flow used to derive the theoretical RPM. The left side operations are used to derive the elastic properties of the dry rock, whereas the right side steps model the fluid properties. Then the Gassmann model combines the rock and the fluid properties to derive the elastic properties of the saturated rock.

Table 1: The input parameters used in the definition of the theoretical RPM.

Figure 3: Examples of logged elastic properties and calculated petrophysical properties pertaining to a well that reached the reservoir rock. The top of the target gas-sand is located at 2450 m, approximately. From left to right: V_p , V_s , density, water saturation, porosity and shaliness.

Figure 4: Comparison between the actual and the predicted elastic properties by the four RPMs. Density, V_p and V_s are represented in a), b) and c), respectively. The correlation coefficients computed for each approach are shown in d), e) and f) for density, V_p and V_s , respectively.

Figure 5: Rock-physic templates showing the influence of each petrophysical parameter on the P-impedance (I_p) and S-impedance (I_s). Water saturation (S_w), porosity (ϕ) and shaliness (Sh) are represented from left to right. Part a) refers to the actual well-log data, whereas parts b), c), d) and e) refer to the elastic properties predicted by the SR, NN, TRPM and GA methods, respectively. In part a) the hydrocarbon trend is indicated by the black arrow.

Figure 6: Graphical representations of the rock-physics models derived by step-wise regression, neural network, theoretical rock physics model and genetic algorithms are, respectively, shown in a), b), c) and d). These surfaces represent the V_s variations as a function of the shale content and the porosity, keeping fixed the depth and the water saturation to 2600 m and to 50%, respectively.

Figure 7: Graphical representations of the rock-physics models derived by step-wise regression, neural network, theoretical rock physics model and genetic algorithms are, respectively, shown in a), b), c) and d). These surfaces represent the V_p variations as a function of the water saturation and the porosity, keeping fixed the depth and the shaliness to 2600 m and to 20%, respectively.

Figure 8: Graphical representations of the rock-physics models derived by step-wise regression, neural network, theoretical rock physics model and genetic algorithms are, respectively, shown in a), b), c) and d). These surfaces represent the density variations as a function of the shaliness and the porosity, keeping fixed the depth and the water saturation to 2600 m and to 50%, respectively.

Figure 9: Results of the blind test. V_p , V_s and density are represented in a), b) and c), respectively. The correlation coefficients computed for each approach are shown in d), e) and f) for V_p , V_s and density, respectively.

Figures and Tables

Figure 1

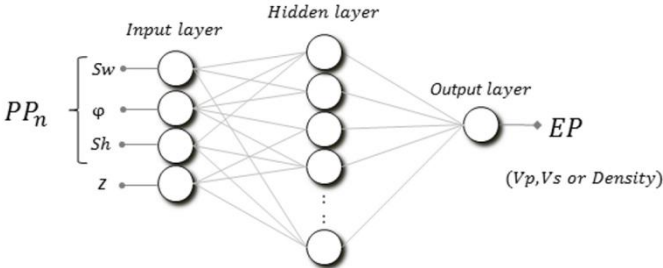


Figure 2

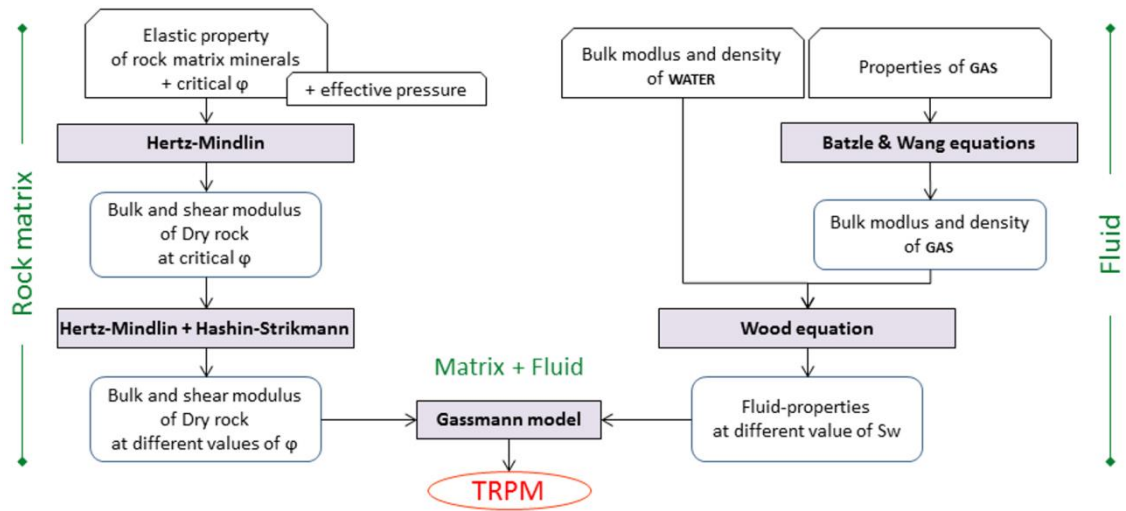


Table 1

<i>Quartz bulk modulus</i>	37 GPa
<i>Quartz shear modulus</i>	39 GPa
<i>Quartz density</i>	2650 Kg/m ³
<i>Clay bulk modulus</i>	13 GPa
<i>Clay shear modulus</i>	2 GPa
<i>Clay density</i>	2380 Kg/m ³
<i>Shale critical porosity</i>	70 %
<i>Sand critical porosity</i>	40 %
<i>Coordination number</i>	7
<i>Brine bulk modulus</i>	2.25 GPa
<i>Brine density</i>	1045 Kg/m ³
<i>Specific gas density</i>	0.9
<i>Temperature at the target depth</i>	65 °C

Figure 3

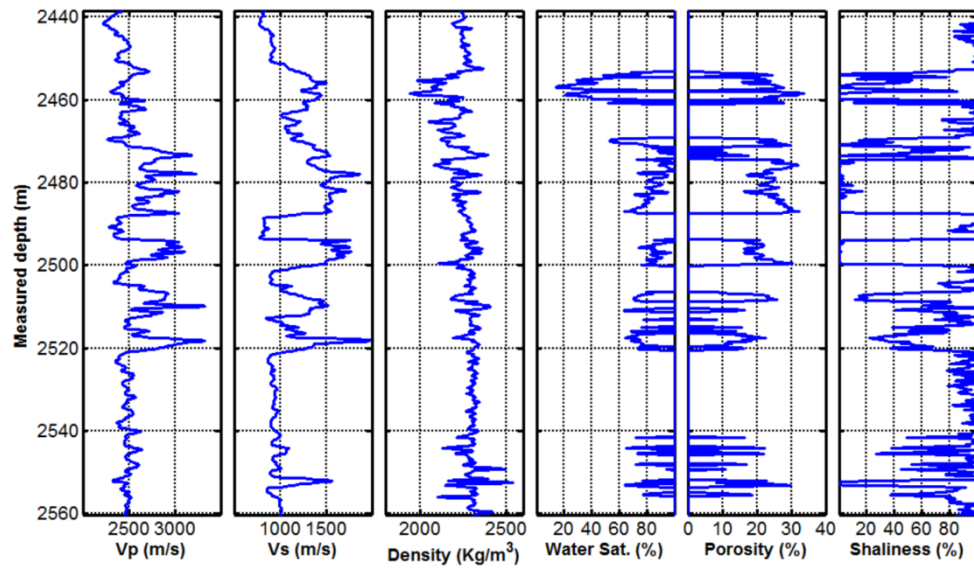


Figure 4

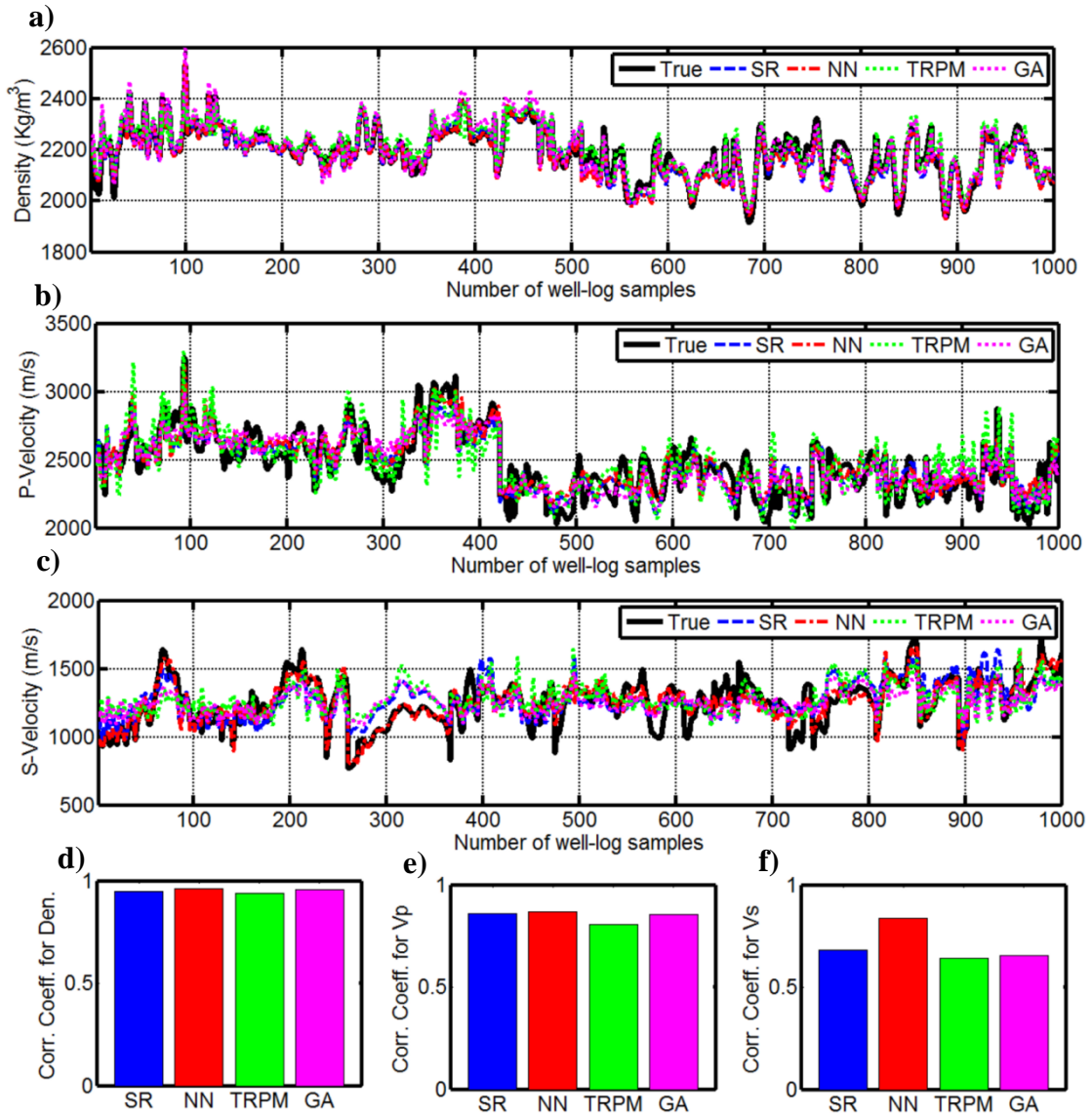


Figure 5

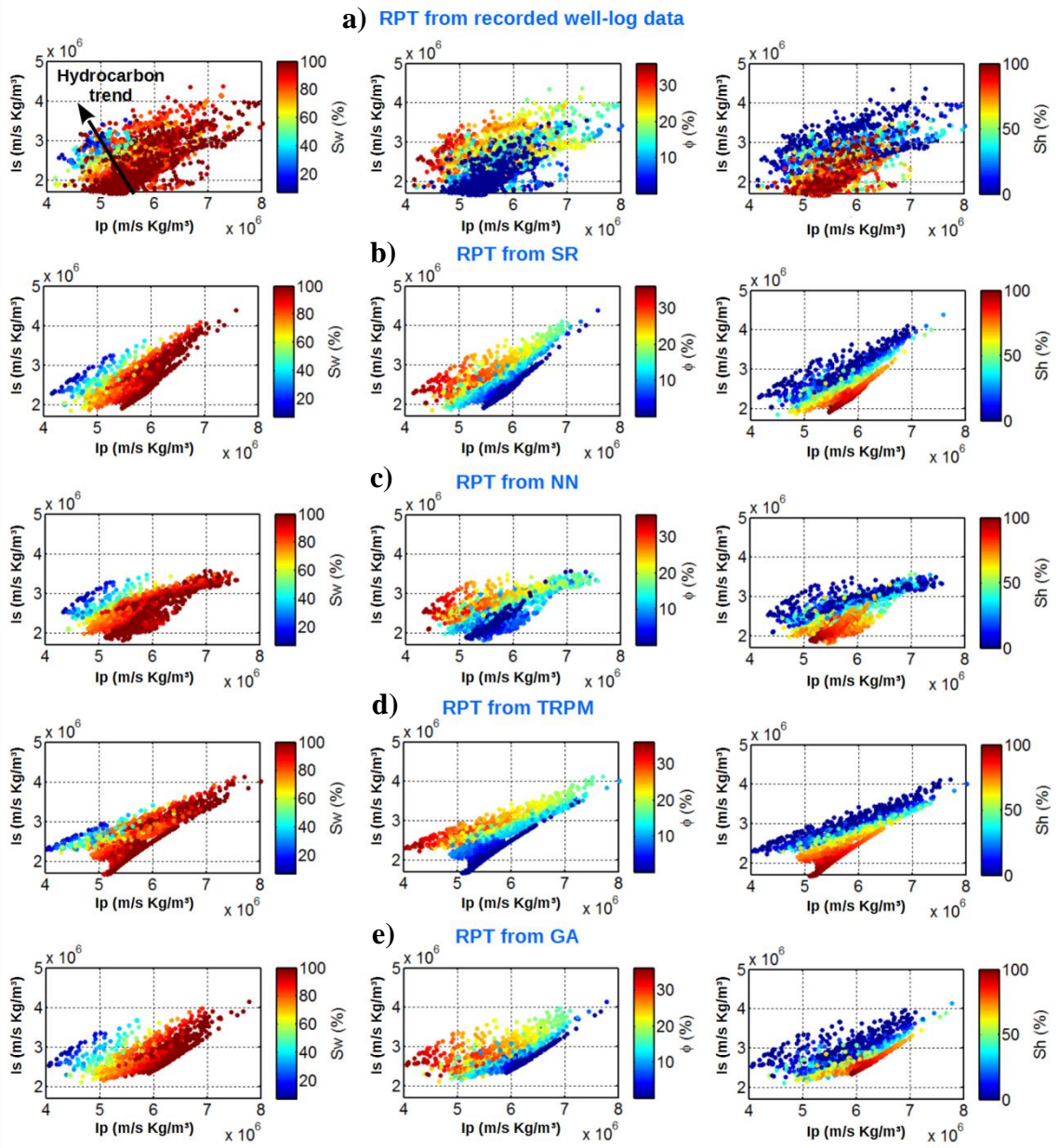


Figure 6

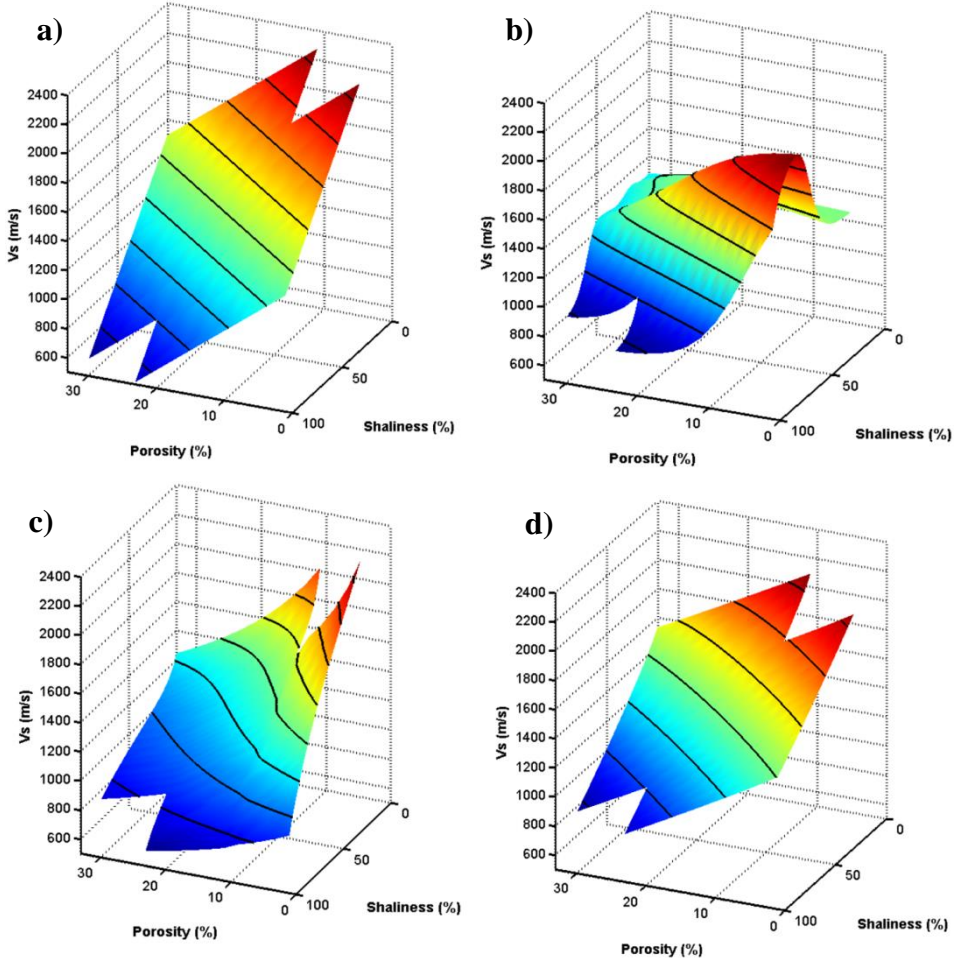


Figure 7

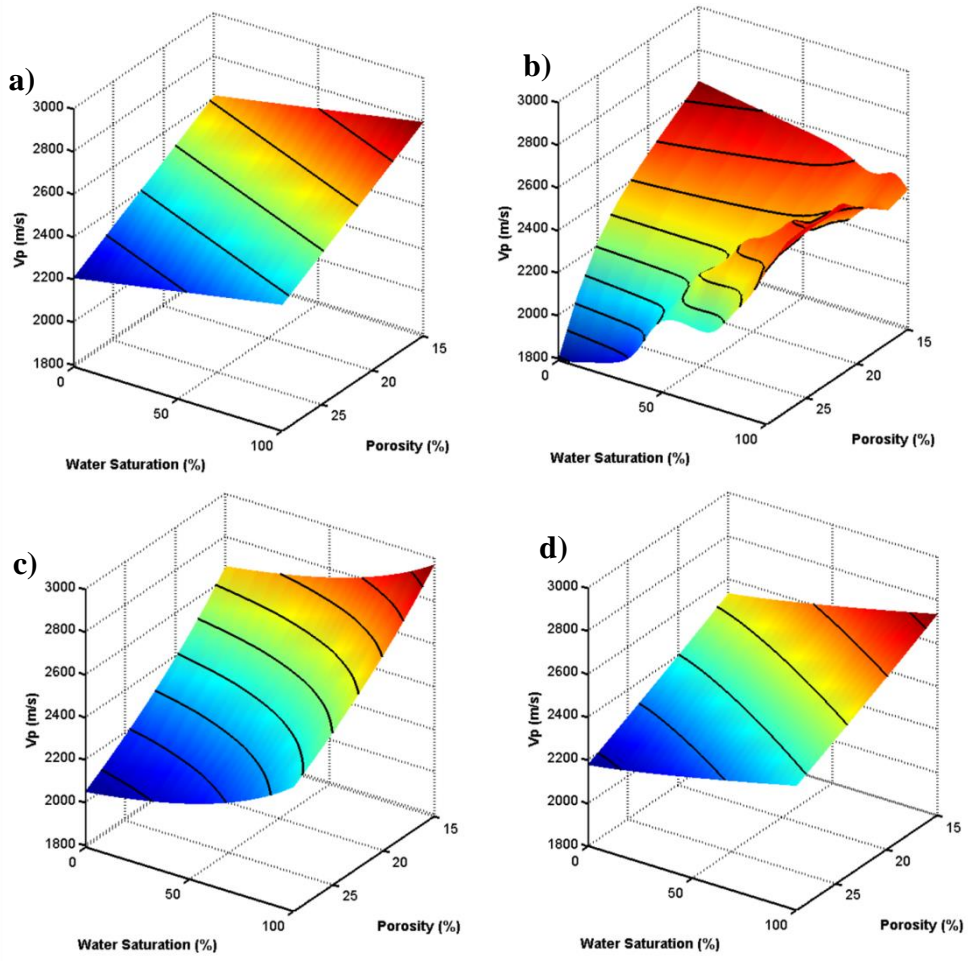


Figure 8

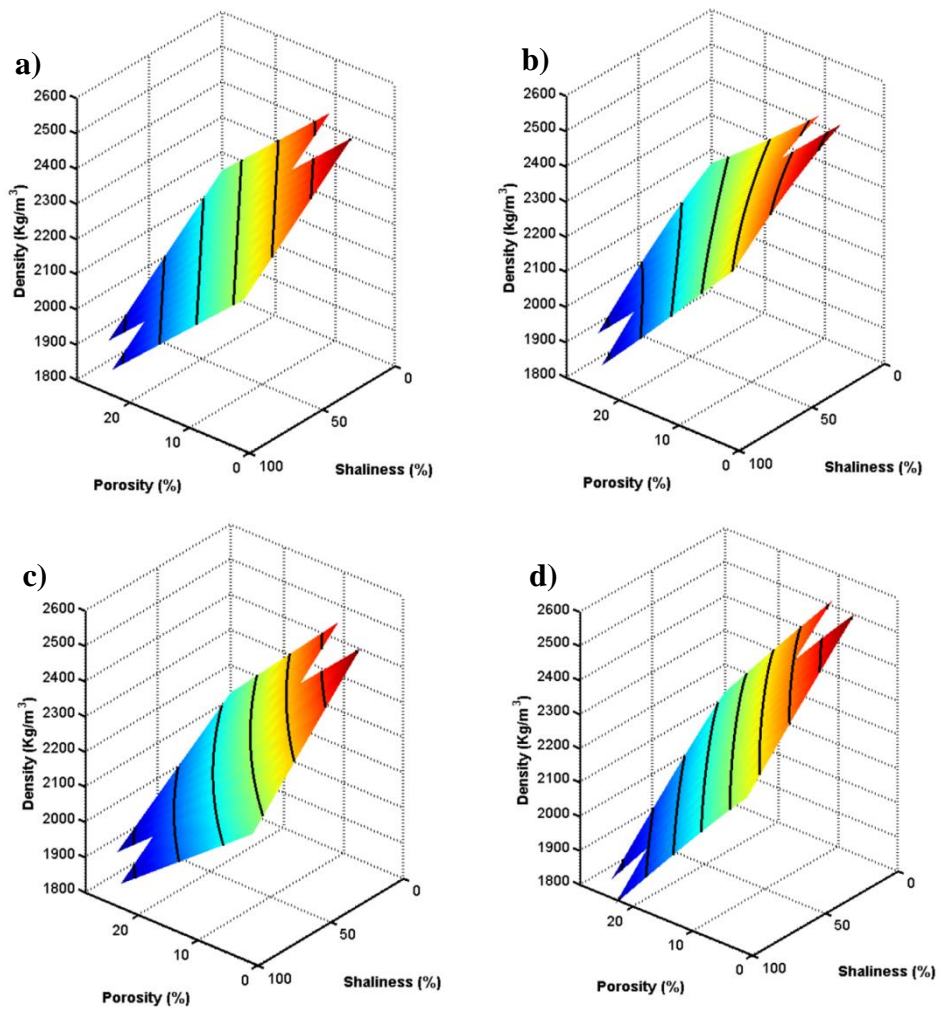


Figure 9

